Cancellation of OpAmp Virtual Ground Imperfections by a Negative Conductance applied to improve RF Receiver Linearity

Dlovan H. Mahrof, Eric A.M. Klumperink, Zhiyu Ru, Mark S. Oude Alink, and Bram Nauta

University of Twente, IC Design group, Enschede, The Netherlands

Contact Information:
Name: Dlovan Hoshiar Mahrof
Address: Twente University, Carré 2635, P.O. Box 217, 7500 AE Enschede, Netherlands
Phone: +31 683 718 565, Fax: +31 53 489 1034, E-mail: d.h.mahrof@alumnus.utwente.nl

---

Abstract **— High linearity CMOS radio receivers often exploit linear V-I conversion at RF, followed by passive down-mixing and an OpAmp-based Transimpedance Amplifier at baseband. Due to nonlinearity and finite gain in the OpAmp, virtual ground is imperfect, inducing distortion currents. This paper proposes a negative conductance concept to cancel such distortion currents. Through a simple intuitive analysis, the basic operation of the technique is explained. By mathematical analysis the optimum negative conductance value is derived and related to feedback theory. In- and out-of-band linearity, stability and Noise Figure are also analyzed. The technique is applied to linearize an RF receiver, and a prototype is implemented in 65 nm technology. Measurement results show an increase of in-band IIP_3 from 9dBm to >20dBm, and IIP2 from 51 to 61dBm, at the cost of increasing the noise figure from 6 to 7.5dB and <10% power penalty. In 1MHz bandwidth, a Spurious-Free Dynamic Range of 85dB is achieved at <27mA up to 2GHz for 1.2V supply voltage.**

Index Terms — Receiver linearity, interference robustness, compression, blocking, in-band and out-band IIP_3, IIP_2, mixer-first receiver architecture, transimpedance amplifier (TIA), negative conductance technique, CMOS, wideband base station receiver, software radio, software defined radio, cognitive radio.

I. INTRODUCTION

Linearity requirements on radio receivers become increasingly challenging, as the radio spectrum becomes more crowded. Moreover, there is a trend towards more wideband and more flexible radio hardware with less dedicated RF filtering ("Software Defined Radio"). As an example, Figure 1 plots IIP_3 requirements calculated for E-UTRA for a wideband base station receiver in three scenarios: wide area, local area and home [1]. Apart from the high 100MHz bandwidth, note the sudden step in IIP_3 requirements at the band-edge. Also note that less coverage area (home versus wide area), corresponds to higher in-band IIP_3 but a smaller step to out-of-band IIP_3 (i.e. around 16dB for home area versus 40dB for wide area). As a consequence of the lack of a reasonable transition band, on-chip analog filtering is ineffective to relax the IIP_3 requirement, and off-chip filters are expensive. Depending on the blocker scenario, compression point requirements may or may not be affected. In this paper, we propose a circuit technique that can increase IIP_3 simultaneously for in- and out-of-band, at roughly constant compression point. Receivers with high IIP_3 are also very important for opportunistic dynamic spectrum access via a cognitive radio, as is exemplified in Figure 2 for a Digital TV band. Strong interferers (incumbent TV signals) may be present in directly adjacent channels, again making on-chip RF filtering ineffective. Again, high linearity is required also to prevent cross-modulation effects [2] from desensitizing the receiver. A part from the RF receivers, the spectrum sensing front-end also requires high in-band IIP_3 in order to minimize the errors in detecting the empty channels in the spectrum.

Strong RF interference can easily clip baseband amplifiers, while higher required bandwidths limit the amount of available loop-gain for negative feedback. When pushing linearity, avoiding voltage gain at RF (See Figure 3) is instrumental [[3]-[8]]. Exploiting RF V-I conversion followed by passive down-mixing and then simultaneous I-V conversion and filtering at IF/baseband with OpAmps, an out-of-band IIP_3 of up to +18dBm has been shown [[3],[4]]. Passive mixer-first architectures can even achieve up to +25dBm out-of-band IIP_3 [7]. However in-band IIP_3 is much worse, certainly at high gain. The best in-band IIP_3 results that we found for receivers were +3.5dBm for [3] at 34dB gain and +11dBm for [6] at

19dB gain. Analysis shows that finite OpAmp gain can be a bottleneck, as a non-zero virtual ground node voltage can result in distortion currents. In [9], we recently proposed to exploit a negative conductance technique to cancel distortion currents. In this way, the design of the OpAmp is relaxed and its performance no longer needs to be a bottleneck. The use of a negative conductance has been proposed in [10] to realize TIA flicker noise shaping. Paper [10] also briefly mentions linearity improvement, but linearity benefits were not the focus there. In this paper we will analyze the benefits of a negative conductance, compare analysis to measurements and report some extra experimental results in addition to [9]. Section II presents an intuitive model to understand the basic distortion cancellation concept. Additionally, the optimum negative conductance value is derived by mathematical analysis and related to negative feedback theory. Section III analyses stability issues related to this negative conductance technique. A receiver design, in which the concept is exploited, is discussed in Section IV. The receiver noise figure analysis including the negative conductance contribution is discussed in section V. The analysis is verified by measurements in section VI, while results are also benchmarked to other high linearity receivers. Finally, section VII presents conclusions.

II. LINEARIZATION CONCEPT

To understand the OpAmp linearity limitation and the distortion cancellation technique intuitively, it is instructive to follow a 4-step approach to analyze what happens at the virtual ground node “VGND”, as illustrated in Figure 4 to Figure 8:

Step 1: Assume the RF V-I conversion and mixing are perfectly ideal (i.e. linear and infinite current source resistance for GM), we can use the equivalent baseband model in Figure 4 (omitting the downconversion for simplicity). Assuming a 2-tone input signal $V_S(f)$, the injected current $I_S(f)$ to the VGND node is linear, so without IM_3 tones. Now, if the OpAmp handles large signals at a high but finite gain, its output stage will produce IM_3 products at the OUT node, i.e. $V_{OUT}(f)$. However, as $I_S(f)$ has no IM_3 and the feedback resistor R_F is linear, the voltage over R_F does not contain IM_3 (assuming negligible

OPAMP input current). Consequently, the IM_3 products of $V_{VGND}(f)$ are in absolute sense equal to those of $V_{OUT}(f)$ both in magnitude and phase. Let's denote this "IM_3 copy" effect in Figure 4 as "problem A". Note that the two main tones of $V_{VGND}(f)$ are much smaller than that of $V_{OUT}(f)$, as the ratio $V_{OUT}(f)/V_{VGND}(f)$ for linear terms is equal to the loop gain. As a consequence the ratio between the linear terms and the IM_3 products at VGND node is *much worse* than at the OUT node, causing a more serious problem discussed next.

Step 2: Assume we add a finite output resistance R_O as shown in Figure 5. The nonlinear voltage $V_{VGND}(f)$ over R_O now generates a nonlinear current $I_O(f)$, and hence $I_F(f)$ becomes nonlinear. This current is absorbed by the OpAmp output stage and increases IM_3 at both $V_{OUT}(f)$ and $V_{VGND}(f)$. We will denote this "R_O loading" effect on the VGND node in Figure 5 as "problem B".

Step 3: Once one realizes the main cause for distortion current is $V_{VGND}(f)/R_O$, it is easy to verify that adding a negative conductance with value $G_O=1/R_O$ between VGND and ground can be a solution (see Figure 6). The negative conductance senses V_{VGND} and generates a copy of the distorted current $I_O(f)$, which now flows in a "local circle" via the ground. Consequently, the current injected to the VGND node becomes linear again and we are back at the circuit of problem A, having solved problem B.

Step 4: Still, the OpAmp output voltage contains some IM_3, equal to that on the VGND node. By slight overcompensation this IM_3 contribution can also be cancelled. To show this, it is useful to model the floating resistor R_F with an equivalent network consisting of four single-ended linear transconductor blocks G_F ($G_F=1/R_F$), all referred to ground as shown in Figure 7 (a). The two shorted G_F blocks, indicated with a dashed ellipse, can be replaced by a simple R_F resistor to the ground (see Figure 7 (b)). Thus Figure 7 (c) results with $R_{F\text{-}VGND}$ and $R_{F\text{-}OUT}$, (loading resistances at the VGND node and the OUT node, respectively), $G_{F\text{-}VGND}$ (the transconductance sensing V_{OUT} and injecting current to the VGND node), and $G_{F\text{-}OUT}$ (the transconductance sensing V_{VGND} and injecting current to the OUT node). We assigned different names to G_F and R_F blocks in order to distinguish between their effects on nonlinearity

at the VGND node and the OUT node separately. Figure 7 (c) clearly shows the loading effect of R_F (i.e. $R_{F\text{-}VGND}$) at the VGND node. Now, when the negative conductance cancels this loading effect (see Figure 8), the injecting current of $G_{F\text{-}VGND}$ becomes equal to the linear current I_S. As $V_{OUT}=I_S/G_{F\text{-}VGND}=-I_S.R_F$, the OpAmp output voltage V_{OUT} becomes linear. This way problem A is solved as well.

Overall, combining the solutions for problem A and B, the optimal total negative conductance is: $G_{TOTAL}=1/R_O+1/R_F$. To mathematically prove this optimum cancellation condition, the OpAmp (see Figure 9) is modeled as an OTA with nonlinear transconductance and also a nonlinear output resistance because we aim for high output swing:

$$I_F = gm_1 V_{IN} + gm_3 V_{IN}^{\ 3} + go_1 V_O + go_3 V_O^{\ 3} \tag{1}$$

In the model, we assume that the third order nonlinearities are more pronounced than the second order nonlinear terms, which is reasonable considering the OpAmp will be implemented in fully differential form. In the Appendix A, the nonlinear relation between V_{OUT} and signal current I_S is derived using the model in Figure 9. It can be expressed in terms of a linear (Ω_1) and third-order nonlinear (Ω_3) coefficient:

$$V_{OUT} = \Omega_1 I_S + \Omega_3 I_S^{\ 3} \tag{2}$$

The linear coefficient Ω_1 is the I/V conversion gain:

$$\Omega_1 = \frac{1}{\left[\frac{1}{a}\left(\frac{1}{R_O} + \frac{1}{R_{F-VGND}}\right) + G_{F-VGND}\right]} \tag{3}$$

Where (a) is a function of the linear terms of the OpAmp model (i.e. gm_1, go_1) and the R_F effects at the OUT node (i.e. $R_{F\text{-}OUT}$ and $G_{F\text{-}OUT}$). For very high gm_1, (a) reaches $-\infty$. Consequently, the I/V conversion gain of (3) becomes $1/G_{F\text{-}VGND}= -R_F$.

The third-order distortion coefficient (Ω_3) is:

$$\Omega_3 = \frac{NL_3\left(\frac{1}{R_O}+\frac{1}{R_{F-VGND}}\right)}{\left[\frac{1}{a}\left(\frac{1}{R_O}+\frac{1}{R_{F-VGND}}\right)+G_{F-VGND}\right]^4} \quad (4)$$

where (*NL_3*: see Appendix A) is related to the nonlinear terms of the OpAmp model and is a function of (i.e. gm_1, gm_3, go_1 and go_3) and the effect of R_F on the OUT node (i.e. $R_{F\text{-}OUT}$ and $G_{F\text{-}OUT}$). Now, if the *negative conductance technique cancels $1/R_O+1/R_{F\text{-}VGND}$* from (3) and (4) we see that Ω_1 reaches $1/G_{F\text{-}VGND}=-R_F$ and Ω_3 becomes zero (distortion is cancelled). Note that since the voltage swing at the VGND node is small, the effect of negative conductance nonlinearity can be very small.

The linearity benefit can also be verified by applying feedback theory to Figure 9 as shown in Figure 10, excluding GM. The feedback topology of the circuit is Voltage-Current Feedback [11]. The output voltage (i.e. V_{OUT}) is sensed and converted to a proportional feedback current βV_{OUT}, where $\beta=G_{F\text{-}VGND}$ (in Siemens). This feedback current is subtracted from the input current I_S resulting in an error current $I_{error}=I_S-\beta V_{OUT}$ to be amplified by the block A. Here, $A=V_{OUT}/I_{error}$, where A has the dimension of a transimpedance [Ω]. It consists of all the blocks of Figure 9, excluding GM and $G_{F\text{-}VGND}$. Actually for finite A, there will be a non-zero I_{error} due to the loading effect of R_O and $R_{F\text{-}VGND}$ on the VGND node. Now the negative conductance increases the input impedance of the A block to infinity by cancelling R_O and $R_{F\text{-}VGND}$, so that I_{error} becomes zero and $A=V_{OUT}/I_{error}$=infinity. Consequently, loopgain Aβ goes to infinity and V_{OUT}/I_S achieves its ideal value $1/\beta=R_F$, i.e. perfect linearity. We conclude that the negative conductance technique increases the loop gain by increasing the value of A. Also note that only a finite value for G_O is needed to make the loopgain theoretically approach infinity, which is not possible by increasing gm_1 in the gain block. Although the feedback theory puts the application of a negative conductance technique in the right context, however the problem with control theory is that it assumes blocks with unilateral operation, which are sometimes not easy to identify (e.g. see Figure 10: feedback

resistor R_F which is supposed to realize the β block also becomes part of the A block). In compare to the feedback analysis, our analysis explains in a simple way how IM_3 is affected by R_O and R_F.

To verify the OpAmp model, we fitted the model derived above to simulations done for the OpAmp that will be introduced later in this paper. Figure 11 shows a close agreement.

Now, before we proceed with detailed circuits design, we will first deal with a potential caveat of negative conductance: the risk of instability.

III. STABILITY ANALYSIS

We will consider two stability aspects: 1) the risk of oscillation, based on a small signal model, and 2) the risk of latch-up. Let us first look at the small signal behavior, referring to Figure 12. As the low-pass filtering is desired, C_F is added as feedback capacitor. Capacitor C_T models the total input capacitance to ground of the OpAmp $C_{IN\text{-}OpAmp}$ and other capacitance C_O at the VGND node (see Figure 3). For simplicity, the OTA is modeled as a frequency dependent transconductance with a dominant pole at ω_O and infinite output impedance:

$$gm(s) = \frac{gm_O}{1 + \frac{s}{\omega_O}} \tag{5}$$

Assuming no further loading at the OUT node, looking into the VGND node (see Figure 12), the impedance (Z_{IN}) consists of the reactance of C_T in parallel to 1/gm(s):

$$Z_{IN} = \frac{1}{s\,C_T} // \frac{1}{gm(s)} = \frac{1}{s\,C_T} // \left[\underbrace{\frac{1}{gm_O}}_{\text{Resistance}} + \underbrace{\frac{s}{gm_O\,\omega_O}}_{\text{Inductance (L)}} \right] \tag{6}$$

Therefore, a parallel RLC tank is seen looking into the VGND node. If the negative conductance would both cancel $1/R_O$ and gm_O, then oscillation would happen at a resonance frequency that depends on the

value of C_T and L (i.e. $f_{res}=1/(2\pi\sqrt{C_T L})$). However, note that the typical virtual ground impedance $1/gm_O$ will normally be much lower than R_O and R_F. Thus, as the negative conductance G_{Total} is designed to cancel $1/R_O$ and $1/R_F$, the point of small signal instability can be designed to be safely far away.

Let's now look at the potential of latch-up of the OpAmp for a case that the negative conductance is too strong, i.e. it produces more current than needed after compensating the current in R_O. As shown in Figure 13, the negative conductance injects current via R_F (i.e. $V_{VGND}G_{Latch\text{-}up\text{-}Risk}$) that needs to be handled by the OpAmp output stage in addition to the main current coming from GM (i.e. I_S):

$$\begin{aligned} I_{OpAmp\text{-}Latch\text{-}up\text{-}Risk} &= I_S + V_{VGND} G_{Latch-up-Risk} \\ &= I_S + \frac{1}{\left[\left(\frac{1}{R_{F-VGND}} - G_{Latch-up-Risk}\right) + a\, G_{F-VGND}\right]} I_S G_{Latch-up-Risk} \end{aligned} \quad (7)$$

Where the relation between V_{VGND} and I_S is derived in Appendix B. Referring to Figure 13 and substituting $G_{Latch\text{-}up\text{-}Risk}=(1/R_F)+\Delta G$, in (7) gives the following relation:

$$I_{OpAmp\text{-}Latch\text{-}up\text{-}Risk} = I_S\left[1 - \frac{\Delta G + \frac{1}{R_F}}{\left(\Delta G + \frac{a}{R_F}\right)}\right] \quad (8)$$

The OpAmp output stage current flows throw R_F and make a voltage drop. The peak of this voltage drop is around $VDD/2\text{-}V_{OpAmpOutputStage\text{-}OV}$, where $V_{OpAmpOutputStage\text{-}OV}$ is the over drive voltages of the OpAmp output stage transistors. Hence, if very strong negative conductance has been used (i.e. high ΔG in (8)), then the current of (8) becomes higher than the OpAmp output stage current capability and the latch-up occur.

IV. RECEIVER DESIGN

We will now apply the negative conductance idea to a high linearity zero-IF radio receiver architecture of Figure 3. To demonstrate the linearity potential of this technique, we will replace the active V-I conversion by a more linear fully passive mixer with resistors in series [4], as shown in Figure 14. Figure 15 shows the complete front-end IC schematic including the negative conductance. Using the equivalent model in Figure 5, we can model the RF part of each branch in I and Q as a grounded resistor R_O and a transconductor GM referred to ground as denoted in Figure 15. However, as resistor R_{RF} is in series with the mixer on-resistance $R_{ON\text{-}MIXER}$ and the virtual ground impedance R_{VGND} of the OpAmp, the equivalent GM now equals $1/(R_{RF}+R_{ON\text{-}MIXER}+R_{VGND})$. This is chosen to be 20mS to realize RF input impedance matching of 50Ω, assuming perfect non overlapping 25% duty-cycle clocks, so the RF-input continuously sees a conduction path to ground. The equivalent output impedance of the mixer at baseband now is $R_O=2(R_{BalUn}+R_{RF}+ R_{ON\text{-}MIXER})$, where the factor 2 is due to the quadrature mixer with 25% duty cycle, connecting each I and Q baseband part to RF two times per LO cycle. To understand this point, let's derive R_O from the power that is delivered by a test voltage source (i.e. $V_{test}=V_a \cos(\omega_{LO}t)$) "looking back" in R_O as shown in Figure 16. This source is connected to the first branch of the I-path. The current I_{test} will flow through $R_{ON\text{-}MIXER}+R_{RF}+R_{BalUn}$ two times LO-cycle, hence we get:

$$P = \frac{1}{T_{LO}}\left[\int_0^{\frac{T_{LO}}{4}} V_{test} I_{test} dt + \int_{\frac{T_{LO}}{2}}^{\frac{3T_{LO}}{4}} V_{test} I_{test} dt\right] = \frac{V_a^{\,2}}{4\left(R_{ON\text{-}MIXER} + R_{BalUn} + R_{RF}\right)} \tag{9}$$

This power must be equal to the power dissipation in R_O:

$$P = \frac{1}{T_{LO}} T_{LO} \int_0^{T_{LO}} \frac{V_{test}^{\,2}}{R_O} dt = \frac{V_a^{\,2}}{2R_O} \tag{10}$$

By equating (9) and (10), the following R_O is derived:

$$R_O = 2\left(R_{ON\text{-}MIXER} + R_{BalUn} + R_{RF}\right) \quad (11)$$

In the derivation of R_O, the power is only balanced with the fundamental, while the effect of the 3rd and higher harmonics are neglected due to the existence of C_O (see Figure 15).

Now, the 50Ω input impedance matching is implemented as a combination of series resistances R_{RF}≈12Ω, the up-converted impedances of the passive mixer switches $R_{ON\text{-}MIXER}$≈28Ω plus the VGND impedance R_{VGND}≈7Ω. The passive mixer consists of simple NMOS switches. C_O=8pF effectively shorts the LO leakage and high IF frequency components to ground. The TIA consists of a class-A input stage and a class-AB output stage, to maximize output swing (see Figure 17, [12] and [3]). Common mode feedback ensures biasing at VDD/2. The feedback impedance is R_F=1.5kΩ and C_F=8pF, to obtain 26dB voltage gain and a -3dB-bandwidth of 12MHz. The differential topology allows for a simple differential implementation of the negative conductance (right part of Figure 15) and high IIP_2. To be able to measure what is the effect of different negative conductance values, $-G_O$ is implemented as a parallel array of identical "unit-transconductors", digitally controllable via multiplier M, with transconductance steps of 0.2mS. Thus M=28 renders G_O=5.6mS to compensate the nominal value of R_O=180Ω ($R_O=2(R_{BalUn}+R_{RF}+R_{ON\text{-}MIXER})=2(50+12+28)=180\Omega$).

We will now consider the noise degradation resulting from the introduction of the negative conductance. Actually this noise can be cancelled by a noise cancellation path [[13],[4]], however this is expected to result in a linearity bottleneck in the auxiliary noise cancellation path. Hence we will analyze the noise figure degradation and aim for minimizing the noise penalty.

V. Noise Figure Analysis (NF)

Receiver topologies with a passive mixer and transimpedance amplifier (TIA), can suffer from amplification of OpAmp noise [14]. The output referred OpAmp noise contribution can be written as:

$$\overline{V_{n-OUT}^2} = \left(1+\frac{R_F}{R_O}\right)^2 \overline{V_{n-OpAmp}^2} \tag{12}$$

Where $V_{n\text{-}OpAmp}$ refers to the (equivalent) input noise voltages of the OpAmp, R_O and R_F are as used in Figure 5. For our design R_F=1.5kΩ and R_O=180Ω, then the amplification factor is equal to $(1+R_F/R_O)^2$=87. Often a high RF V/I conversion (GM-value) is used to achieve an overall noise figure around or below 3dB. Here we will use 20mS, the value desired for input impedance matching. Figure 18 shows a baseband model of Figure 14 with noise sources added. The noise of GM is represented by the current noise source ($I_{n\text{-}Ro}$) of R_O. The noise of R_F is modeled via voltage noise source $V_{n\text{-}RF}$, while $I_{n\text{-}GTotal}$ represents the current noise source of the negative conductance. For simplicity, the OpAmp is modeled as a simple Transconductance (gm). To analyze the noise contributions of $I_{n\text{-}Ro}$ and $I_{n\text{-}GTotal}$ to the output voltage, Ω_1 (i.e. the I/V conversion of the TIA (3)) is useful. The straightforward NF analysis shows:

$$NF = 1+\frac{1}{\left(\frac{1}{2}\Omega_1 GM\right)^2 R_S}\left[\underbrace{\Omega_1{}^2\left(\frac{1}{R_O}+\gamma\, G_{Total}\right)}_{\text{First Term}}+\underbrace{\frac{\overline{V_{n-OpAmp}^2}}{\overline{I_{n-R_O}^2}}\frac{1}{R_O}\left(1+R_F\left(\frac{1}{R_O}-G_{Total}\right)\right)^2}_{\text{Second Term}}+\underbrace{R_F\left(\frac{1}{gm\,R_F}-1\right)^2}_{\text{Third Term}}\right] \tag{13}$$

The first term between the square brackets in (13) shows that the negative conductance G_{Total} has a direct noise contribution to the output. Its noise contribution is scaled by $\gamma/\left(\left(\frac{1}{2}GM\right)^2 R_S\right)$. The "noise excess factor" γ can be minimized to around 2/3 (i.e. theoretically) by choosing a non-minimum channel length for the negative conductance transistors. Long-channel transistors are preferred for 1/f noise. We used 1µm channel length in this design. The second term is the mentioned amplification factor (12) of OpAmp noise including the negative conductance effect (G_{Total}). It is interesting to observe that this term reaches zero when the negative conductance reaches G_{Total}. However, the direct noise contribution of the negative conductance is much higher than the canceled OpAmp noise contribution, hence the total noise figure of the circuit increases. We verified (13) by noise simulations using the OpAmp circuit of Figure 17. The NF is increased from 6 to 7.5 dB given that GM is equal to 20mS. Note that it is also possible to apply the

negative conductance in combination with an LNTA with higher GM and hence lower NF. In that case, the negative conductance can be lower, as R_O>1/GM. However, then IIP_3 of the LNTA becomes a bottleneck.

VI. MEASUREMENT RESULTS AND BENCHMARKING

Figure 19 shows a photo of the implemented 65nm IC. The active area is < 0.2 mm^2 including the clock circuit. Thick metal was used for R_{RF} for high linearity and low spread.

The front-end achieves 26 dB gain (BalUn losses are de-embedded) at 1 GHz LO, over 24MHz bandwidth (BW), 12MHz on either side of LO. To demonstrate distortion cancelling, Figure 20 (a) shows the measured in-band IIP_3 at 150kHz tone spacing (f_1=1004.1MHz and f_2=1004.25MHz) vs. M. IIP_3 clearly improves from around +9 dBm to +21 dBm!

The optimum IIP_3 of +21 dBm is located at M = 32, which fits to our theory $G_{Total}=1/R_O+1/R_F=1/1500+1/180=6.22mS$ so M=6.22mS/0.2mS=31 very well. Figure 20 (b) shows the IM_3 curves versus power for three cases: M=0 (off), M=28 (cancelling of I_O, Figure 6) and M=32 (overall optimum IIP_3). Up to -22dBm input power (note: this power is high for an in-band signal), IM_3 improves. The rise of distortion for high input powers > -23 dBm is due to the clipping of the OpAmp output stage to its 1.2V supply. The negative conductance was pushed to instability (i.e. latch-up of OpAmp output stage). This occurs at M=45 (see (8) $\Delta G=\Delta M x 0.2mS$), safely away from the optimum point by $\Delta M=45-32=13$. This shows a close agreement with our explanation in section III and with the simulations in Figure 21, which is done for the circuit of Figure 13. One tone input signal with power of -16 dBm is used. Around this input power, the OpAmp output stage begins to clip. According to our simulation, the latch-up occurs for $\Delta M \geq 14$. The same mechanism, discussed in section II, of this technique also improves IIP_2 by more than 10 dB as shown in Figure 22. Table I compares/summarizes the IIP_2 and IIP_3 improvement for three M settings 0, 28 en 32. Note that the optimum linearity point will vary somewhat with Process, Voltage and Temperature (i.e. PVT). The analysis in this paper gives the relation between

the required negative conductance and the resistance values R_O and R_F, which can be a basis for designing an automatic PVT correction circuit.

Figure 23 provides IIP_3 curves versus the frequency offset Δf, with fixed 3.95MHz in-band IM_3 position. The negative conductance clearly increases the IIP_3 both in- and out-of-band (all-Band) with a worst case IIP_3 >+10 dBm. The reason behind less linearity improvement in the transition band can be understood considering the equivalent circuit earlier derived for stability analysis in Figure 12. The negative conductance cancels only the loading of R_O and R_F. However, gm(s), C_F and C_T introduce frequency dependences. Consequently, the "loading effect" on the VGND node (see Figure 5) becomes frequency dependent and will introduce a phase shift compared with the (frequency independent) current generated by the negative conductance. This results in imperfect cancellation, i.e. less linearity improvement at high frequencies. This may be improved in the future by designing the negative conductance to be frequency dependent as well. Up to 10MHz, in-band IIP_3 is >+20dBm, i.e. >10dB improvement thanks to the negative conductance. Then the IIP_3 declines from 12MHz to 135MHz, on the one hand because the OTA gain and hence its linearity degrades, but on the other hand also because the benefit from cancellation drops (the top line in Figure 23 drops faster, versus Δf, than the bottom line). Note that the out-of-band IIP_3 at Δf > 450 MHz is again high, +18 dBm. This is because at high Δf (i.e. spacing between the carriers) the carriers are filtered due to the low pass filtering by C_F, R_F and C_O, hence less IM_3 products. In this region the negative conductance doesn't result in any benefit anymore.

The compression point (CP) is around -13 dBm (hardly affected by M as shown in Figure 24). Due to the virtual ground, S_{11} is hardly affected by the negative conductance and Figure 25 (a) shows that S_{11} < -25 dB. Noise is more worrisome, but depending on the application some degradation may be acceptable, provided that the overall SFDR still improves (i.e. IIP_3 in dBm should improve more than NF in dB degrades). Figure 25 (b) shows that NF increases from 6.2 dB at M=0 to 7.5 dB at M=32. This result is close to the NF prediction in the previous section. The 1/f corner was around 2MHz.

The current consumption without the negative conductance at 1 GHz LO is 18 mA (including 8mA of clock circuitry (i.e. on-chip drivers and divider)), and 1.6 mA more for M=32. The clock divider frequency range (i.e. also the receiving RF frequency) is 0.2-2.6 GHz, where it consumes 2.8-19 mA. The maximum Gate-Source voltage of the mixer switches is equal to the 1.2V supply. The LO leakage to the RF port is less than -75 dBm. The optimum IIP_3 has been measured for 5 samples. The optimum in-band IIP_3 varies ±1 dB around +21 dBm and the corresponding M varies ±2 around M=32.

Table II benchmarks this work to other state-of-the-art receivers with high linearity and/or SFDR. Our front-end is more linear than [[3],[5]] where active RF blocks are present. Even compared to the mixer-first designs [[6],[7]] we achieve better in-band IIP_3 while our SFDR in 1MHz of 85dB is the highest.

VII. CONCLUSIONS

Due to the strong relationship between linearity and voltage swing, it is challenging to improve linearity in advanced CMOS technologies with low supply voltages. Architectures with RF V-I conversion followed by a passive mixers and an OTA-RC Transimpedance Amplifier perform relatively well. In such architectures, the OpAmp can become the bottleneck, especially for wide channel bandwidth, where the amount of loop gain available for negative feedback is limited. Still high linearity is wanted, not only out-of-band but also in-band, as RF-filtering often is ineffective for close-in interferers. This paper shows how virtual ground imperfections due to OTA nonlinearity lead to distortion currents, which can be cancelled exploiting a negative conductance in parallel to the virtual ground node. Although the technique results in slightly degraded noise figure from 6 to 7.5dB the in-band IIP_3 (and IIP_2) is improved by much more (>10dB), resulting in-band SFDR=85dB in 1MHz bandwidth.

ACKNOWLEDGEMENTS

This research is supported by the Dutch Technology Foundation STW (i.e. the applied science division of the NWO, and the Ministry of Economic Affairs Technology Program). We thank STMicroelectronics for silicon donation and CMP, Andreia Cathelin (STM), Michiel C.M. Soer, Gerard

Wienk and Henk de Vries for their measurement assistance. Special thank goes to Shadi S.T. Youssef and Harish K. Subramaniyan for their discussions and remarks on this work.

APPENDIX

Appendix A

In this section, a 3rd order Taylor approximation of V_{OUT} versus I_S (i.e. $V_{OUT}=V_{OUT}(I_S,I_S^3)$) of the transimpedance amplifier in Figure 9 will be derived. The following procedure will be applied:

1. V_{OUT} is derived as a function of V_{VGND}, V_{VGND}^3 and V_{OUT}^3 ➔ $V_{OUT}=V_{OUT}(V_{VGND},V_{VGND}^3,V_{OUT}^3)$.
2. The resulting relationship is rewritten as a function of V_{VGND} and V_{VGND}^3, by using the definition of the 3rd order Taylor coefficients ➔ $V_{OUT}=V_{OUT}(V_{VGND},V_{VGND}^3)$.
3. The inverse function, V_{VGND} as a function of V_{OUT} and V_{OUT}^3, is written as a 3rd order Taylor function by using the procedure explained in [15] ➔ $V_{VGND}=V_{VGND}(V_{OUT},V_{OUT}^3)$.
4. I_S is rewritten as a function of V_{VGND} and V_{OUT} ➔ $I_S=I_S(V_{VGND},V_{OUT})$.
5. Substituting V_{VGND} of step 3 in I_S of step 4 makes I_S to be a function of V_{OUT} and V_{OUT}^3 ➔ $I_S=I_S(V_{OUT},V_{OUT}^3)$.
6. Finally, by repeating the procedure explained in [15], the function of step 5 is inversed to obtain V_O as a function of I_S and I_S^3 ➔ $V_{OUT}=V_{OUT}(I_S, I_S^3)$.

Step 1 ➔ $V_{OUT}=V_{OUT}(V_{VGND},V_{VGND}^3,V_{OUT}^3)$: We begin the derivation by expressing the feedback current I_F at the VGND node and the OUT node (see Figure 9) as follows:

$$\text{At VGND node: } I_F = \frac{V_{VGND}}{R_{F-VGND}} + G_{F-VGND}V_{OUT} \tag{14}$$

At OUT node: $I_F = -\frac{V_{OUT}}{R_{F-OUT}} - G_{F-OUT} V_{VGND}$ (15)

Referring to the OpAmp nonlinear model, we equate the I_F in (1) to I_F in (15) as follows:

$$gm_1 V_{VGND} + gm_3 V_{VGND}^{\ 3} + go_1 V_{OUT} + go_3 V_{OUT}^{\ 3} = -\frac{V_{OUT}}{R_{F-OUT}} - G_{F-OUT} V_{OUT}$$

$$V_{OUT} = \underbrace{-\frac{(gm_1 + G_{F-OUT})}{\left(go_1 + \frac{1}{R_{F-OUT}}\right)}}_{a} V_{VGND} \underbrace{-\frac{gm_3}{\left(go_1 + \frac{1}{R_{F-OUT}}\right)}}_{b} V_{VGND}^{\ 3} \underbrace{-\frac{go_3}{\left(go_1 + \frac{1}{R_{F-OUT}}\right)}}_{c} V_{OUT}^{\ 3} \quad (16)$$

Step 2 ➔ $V_{OUT}=V_{OUT}(V_{VGND},V_{VGND}^{\ 3})$: V_{OUT} is defined as: $V_{OUT}=\beta_1 V_{VGND} + \beta_2 V_{VGND}^{\ 2} + \beta_3 V_{VGND}^{\ 3}$, which is a 3rd order Taylor approximation around $V_{VGND}=0$, where β_1, β_2 and β_3 are the Taylor coefficients:

$$\beta_{n=1,2,3} = \frac{1}{n!}\left(\frac{\partial^n V_{OUT}}{\partial\ V_{VGND}^{\ n}}\right)\Bigg|_{V_{VGND}=0}$$

To derive β_1, we differentiate (16) with respect to V_{VGND} as follows:

$$\frac{\partial\ V_{OUT}}{\partial\ V_{VGND}} = a + 3bV_{VGND}^{\ 2} + 3cV_{OUT}^{\ 2}\frac{\partial\ V_{OUT}}{\partial\ V_{VGND}} \Rightarrow \frac{\partial\ V_{OUT}}{\partial\ V_{VGND}} = \frac{a + 3bV_{VGND}^{\ 2}}{1 - 3cV_{OUT}^{\ 2}}$$

$$\therefore \beta_1 = \left(\frac{\partial\ V_{OUT}}{\partial\ V_{VGND}}\right)\Bigg|_{V_{VGND}=0} = a = -\frac{(gm_1 + G_{F-OUT})}{\left(go_1 + \frac{1}{R_{F-OUT}}\right)}$$

The same procedure is used to derive β_2 and β_3:

$$\beta_2 = \frac{1}{2}\left(\frac{\partial^2 V_{OUT}}{\partial\ V_{VGND}^{\ 2}}\right)\Bigg|_{V_{VGND}=0} = 0 \quad \text{and} \quad \beta_3 = \frac{1}{6}\left(\frac{\partial^3 V_{OUT}}{\partial\ V_{VGND}^{\ 3}}\right)\Bigg|_{V_{VGND}=0} = b + a^3 c$$

$$V_{OUT} = \underbrace{a}_{\beta_1} V_{VGND} + \underbrace{\left(b + a^3 c\right)}_{\beta_3} V_{VGND}{}^3 \tag{17}$$

Step 3 ➔ $V_{VGND}=V_{VGND}(V_{OUT}, V_{OUT}{}^3)$: We write the inverse of (17) in the Taylor series form: $V_{VGND} =\alpha_1 V_{OUT}+ \alpha_2 V_{OUT}{}^2 +\alpha_3 V_{OUT}{}^3$. Deriving α_1, α_2 and α_3 can be done by the procedure below.

First, let's substitute (17) into its abovementioned inversed form as follows:

$$V_{VGND} = \alpha_1\left(\beta_1 V_{VGND} + \beta_3 V_{VGND}{}^3\right) + \alpha_2\left(\beta_1 V_{VGND} + \beta_3 V_{VGND}{}^3\right)^2 + \alpha_3\left(\beta_1 V_{VGND} + \beta_3 V_{VGND}{}^3\right)^3$$

By equating the right to the left side of the equation above [15], the coefficients α_1, α_2 and α_3 are derived:

$$V_{VGND} = \underbrace{\frac{1}{a}}_{\alpha_1} V_{OUT} \underbrace{- \frac{\left(b + a^3 c\right)}{a^4}}_{\alpha_3} V_{OUT}{}^3 \tag{18}$$

Step 4 ➔ $I_S=I_S(V_{VGND},V_{OUT})$: Referring to I_S in Figure 9, we substitute the I_F (14) at the VGND node in the following equation:

$$I_S = I_O + I_F = \left(\frac{1}{R_O} + \frac{1}{R_{F-VGND}}\right) V_{VGND} + G_{F-VGND} V_{OUT} \tag{19}$$

Step 5 ➔ $I_S=I_S(V_{OUT},V_{OUT}{}^3)$: By substituting (18) into (19), the following equation is obtained:

$$I_S = \left[\frac{1}{a}\left(\frac{1}{R_O} + \frac{1}{R_{F-VGND}}\right) + G_{F-VGND}\right] V_{OUT} - \frac{\left(b + a^3 c\right)}{a^4}\left(\frac{1}{R_O} + \frac{1}{R_{F-VGND}}\right) V_{OUT}{}^3 \tag{20}$$

Step 6 ➔ $V_{OUT}=V_{OUT}(I_S, I_S{}^3)$: Finally, by inversing (20), we reach the following expression:

$$V_{OUT} = \underbrace{\frac{1}{\left[\frac{1}{a}\left(\frac{1}{R_O} + \frac{1}{R_{F-VGND}}\right) + G_{F-VGND}\right]}}_{\Omega_1} I_S + \underbrace{\frac{NL_3\left(\frac{1}{R_O} + \frac{1}{R_{F-VGND}}\right)}{\left[\frac{1}{a}\left(\frac{1}{R_O} + \frac{1}{R_{F-VGND}}\right) + G_{F-VGND}\right]^4}}_{\Omega_3} I_S{}^3 \tag{21}$$

Where: $NL_3 = \frac{\left(b + a^3 c\right)}{a^4}$ is related to the nonlinear terms of the OpAmp model.

Appendix B

In this section, the relation between V_{VGND} and I_S is derived to be used in the latch-up analysis section. In order to simplify this analysis, we assume a linear OpAmp (i.e gm_3=go_3=0). Consequently, (16) and (21) can be simplified as follows:

$$V_{VGND} = \frac{1}{a} V_{OUT} \tag{22}$$

$$V_{OUT} = \Omega_1 I_S \tag{23}$$

Combining (22) and (23), gives the following relation:

$$V_{VGND} = \frac{\Omega_1}{a} I_S = \frac{1}{\left[\left(\frac{1}{R_O} + \frac{1}{R_{F-VGND}}\right) + a\, G_{F-VGND}\right]} I_S \tag{24}$$

After that the negative conductance cancels the loading effect of R_O on the VGND node, it injects current via R_F that needs to be handled by the OpAmp output stage (see Figure 13 and Figure 17). Now if the negative conductance becomes too strong then the potential latch-up becomes a real risk. For the case of latch-up, (24) can be further elaborated to obtain the following equation:

$$V_{VGND} = \frac{1}{\left[\left(\frac{1}{R_{F-VGND}} - G_{Latch-up}\right) + a\, G_{F-VGND}\right]} I_S \tag{25}$$

REFERENCES

[1] 3GPP TS 36.104: "Evolved Universal Terrestrial Radio Access (E-UTRA); Base Station (BS) radio transmission and reception", available online, http://www.3gpp.org.

[2] D. H. Mahrof, E. A. M. Klumperink, J. Haartsen and B. Nauta, "On the effect of spectral location of interfererson linearity requirements for wideband cognitive radio receivers", IEEE Symp. New Frontiers in Dynamic Spectrum Access Networks (DySPAN), pp. 1-9 April 2010.

[3] Z. Ru, E.A.M. Klumperink, B. Nauta, “A Software-Defined Radio Receiver Architecture Robust to Out-of-Band Interference”, ISSCC Dig. Tech. Papers, pp. 230-231, Feb. 2009.

[4] D. Murphy, A. Hafez, A. Mirzaei, M. Mikhemar, H. Darabi, M.F. Chang, A. Abidi, "A Blocker-Tolerant Wideband Noise-Cancelling Receiver with a 2dB Noise Figure", ISSCC Dig. Tech. Papers, pp. 74-76, Feb. 2012.

[5] S.S.T. Youssef, R.A.R. van der Zee, B. Nauta, "Active Feedback Receiver with Integrated Tunable RF Channel Selectivity, Distortion Cancelling, 48dB Stop-Band Rejection and > +12dBm Wideband IIP3, Occupying < 0.06mm2 in 65nm CMOS", ISSCC Dig. Tech. Papers, pp. 166-168, Feb. 2012.

[6] M.C.M. Soer, E.A.M. Klumperink, Z. Ru, F.E. van Vliet, B. Nauta, "A 0.2-to-2.0GHz 65nm CMOS Receiver Without LNA Achieving >11dBm IIP3 and <6.5dB NF", ISSCC Dig. Tech. Papers, pp. 222-223, Feb. 2009.

[7] C. Andrews, A.C. Molnar, “A Passive Mixer-First Receiver With Digitally Controlled and Widely Tunable RF Interface”, IEEE Journal of Solid-State Circuits, vol. 45, no. 12, pp. 2696-2708, Dec. 2010.

[8] S.C. Blaakmeer, E.A.M. Klumperink, D.M.W. Leenaerts, B. Nauta, "The Blixer, a Wideband Balun-LNA-I/Q-Mixer Topology", IEEE Journal of Solid-State Circuits, vol.43, pp.2706,2715, Dec. 2008.

[9] D. H. Mahrof, E. A. M. Klumperink, M. S. Oude Alink, and B. Nauta, “A receiver with in-band IIP3>20dBm, exploiting cancelling of OpAmp finite-gain-induced distortion via negative conductance”, IEEE Radio Frequency Integrated Circuits Symp. (RFIC), pp. 601–604, Jun. 2013.

[10] J. Deguchi et al, “A Fully Integrated 2x1 Dual-Band Direct-Conversion Mobile WiMAX Transceiver With Dual-Mode Fractional Divider and Noise-Shaping Transimpedance Amplifier in 65 nm CMOS”, IEEE Journal of Solid-State Circuits, vol. 45, pp. 2774 - 2784, Dec. 2010.

[11] B. Razavi, *RF Microelectronics*, Prentice Hall, New Jersey, 1998.

[12] Z. Ru, “PhD thesis: Frequency Translation Techniques for Interference-Robust Software-Defined Radio Receivers”, The Netherlands, Twente University, 2009.

[13] F. Bruccoleri, E.A.M. Klumperink, and B. Nauta, ”Noise Cancelling in Wideband CMOS LNAs", ISSCC Dig. Tech. Papers, pp. 406-407, Feb. 2002.

[14] W. Redman-White, D.M.W. Leenaerts, “1/f Noise in Passive CMOS Mixers for Low and Zero IF Integrated Receivers”, ESSCIRC, pp. 18-20, Sep. 2001.

[15] E.A.M. Klumperink, “PhD thesis: Transconductance Based CMOS Circuits”, The Netherlands, Twente University, 1997. online: http://jive.el.utwente.nl/home/erick/Klumperink-PhD-Thesis.pdf

Figure and Table Captions

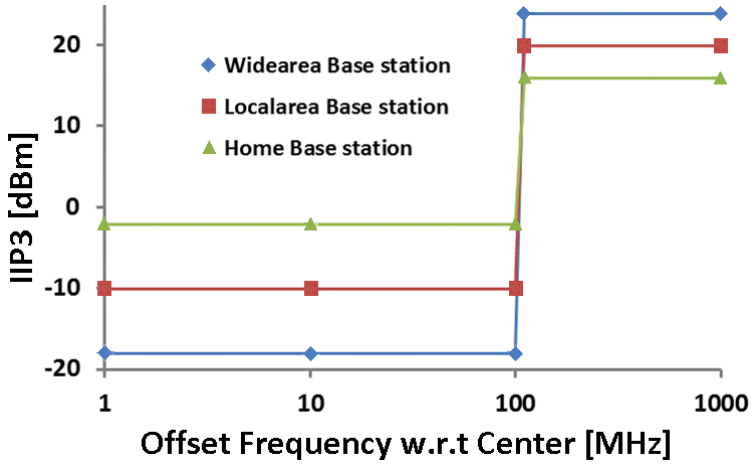

Figure 1: Example IIP_3 requirement for E-UTRA [1]

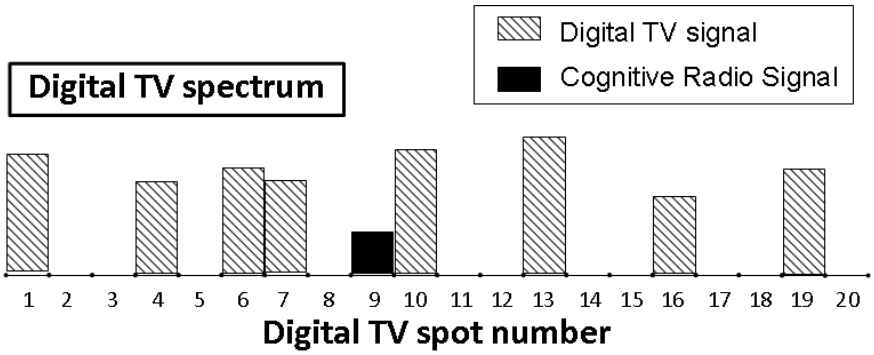

Figure 2: Digital TV spectrum [2] in which a cognitive radio operates in an adjacent channel

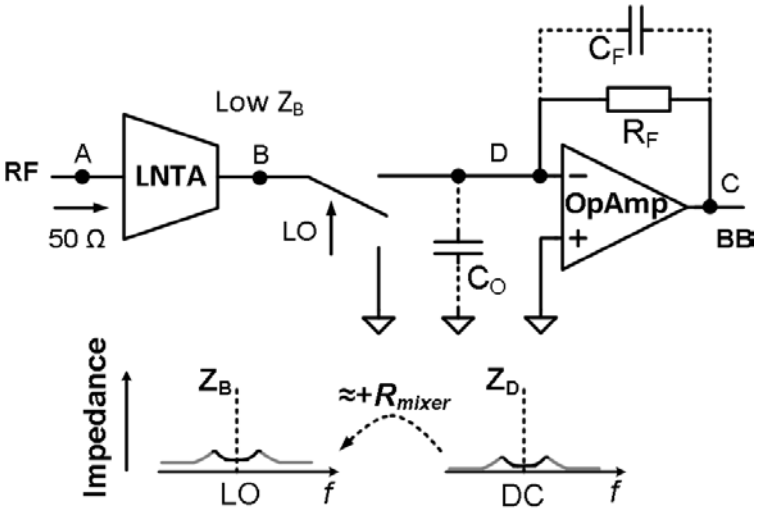

Figure 3: High blocker tolerant linear receiver

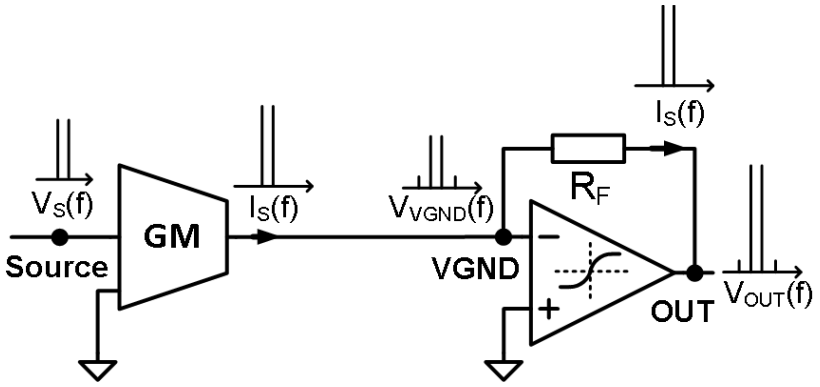

Figure 4: OpAmp nonlinearity problem A: IM_3 is copied from the OUT node to the VGND node

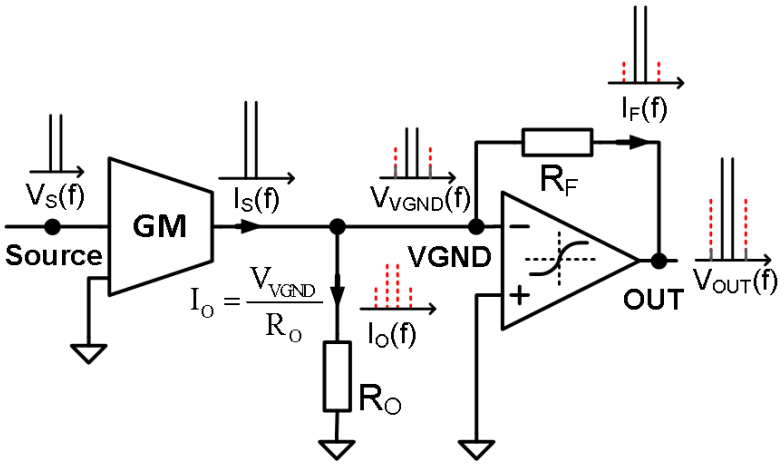

Figure 5: OpAmp nonlinearity problem B: R_O loads the VGND node

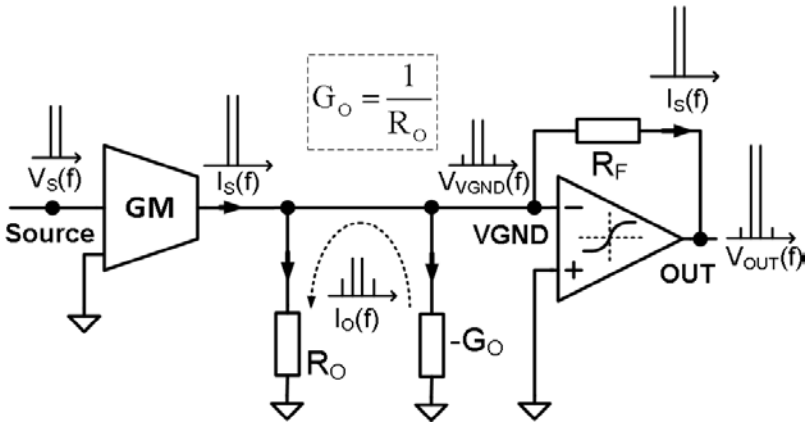

Figure 6: Solving problem B via negative conductance with $G_O=1/R_O$

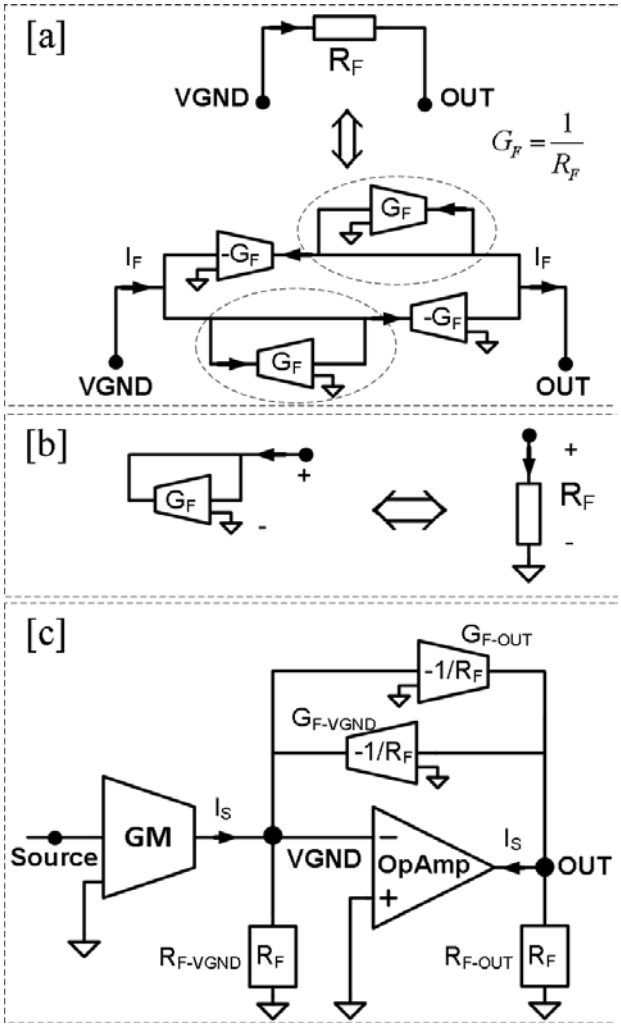

Figure 7: Equivalent model of the effect that R_F has on the OUT node and the VGND node

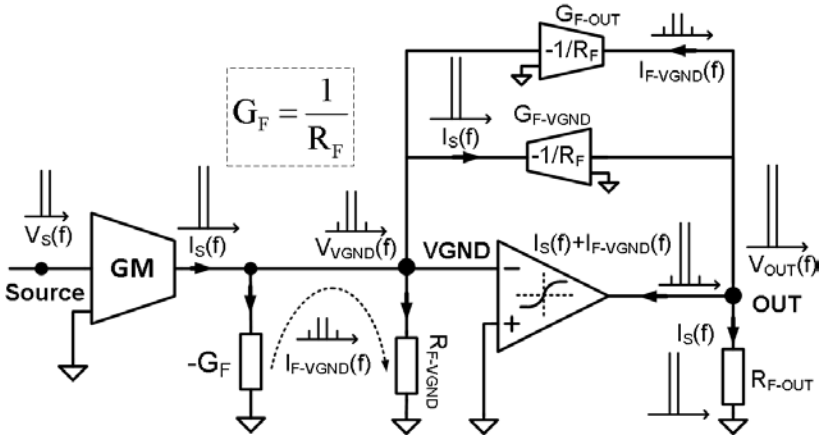

Figure 8: Solving problem A via negative conductance with $G_F = 1/R_F$

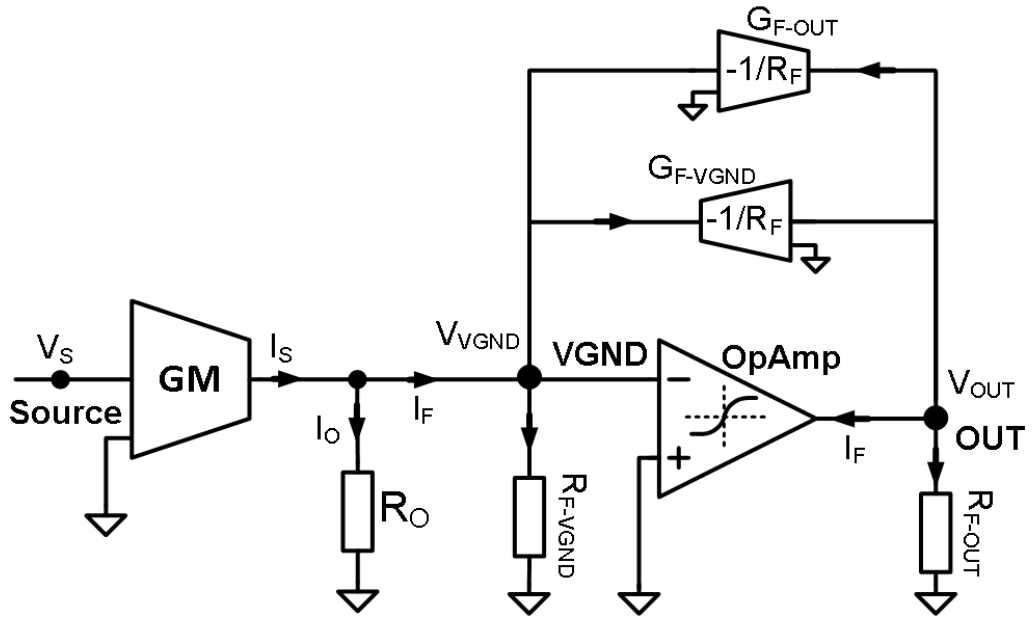

Figure 9: Baseband model with R_O and the extended R_F for nonlinearity derivations

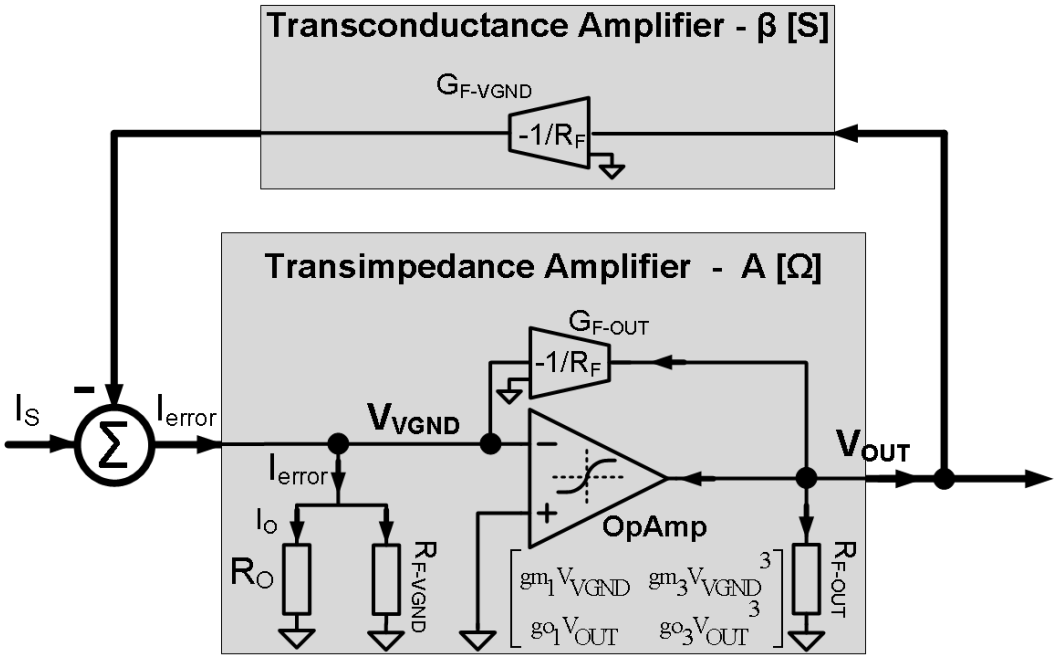

Figure 10: Applying feedback theory to Figure 9, excluding GM

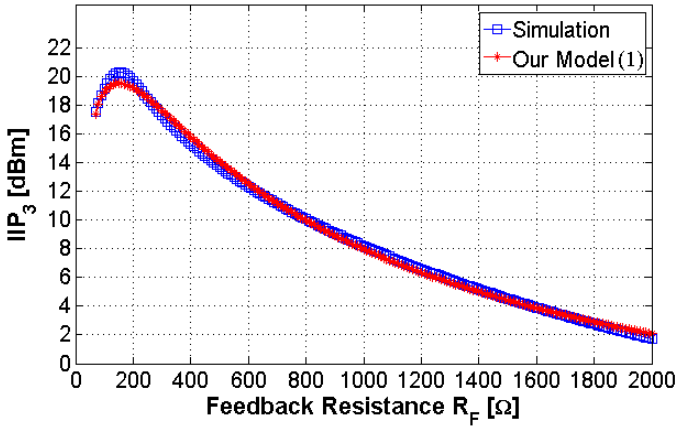

Figure 11: OpAmp model (1) verification

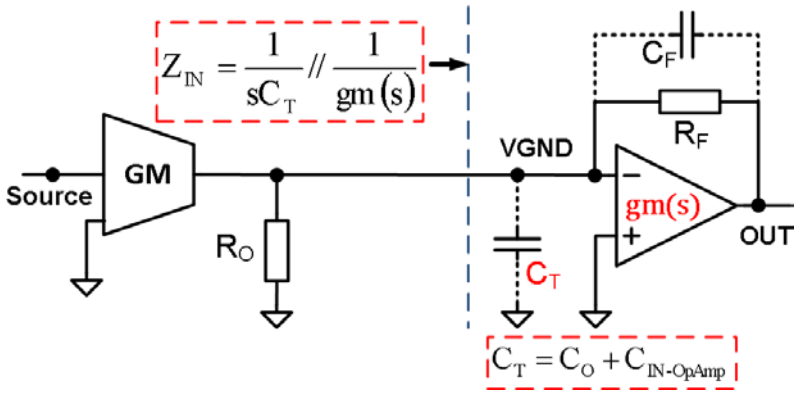

Figure 12: Circuit diagram for small signal stability analysis

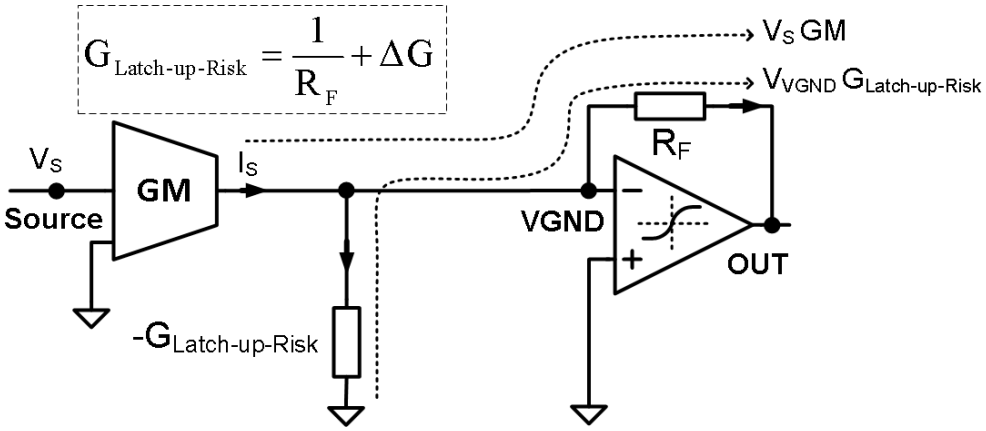

Figure 13: Latch-up problem at the OUT node

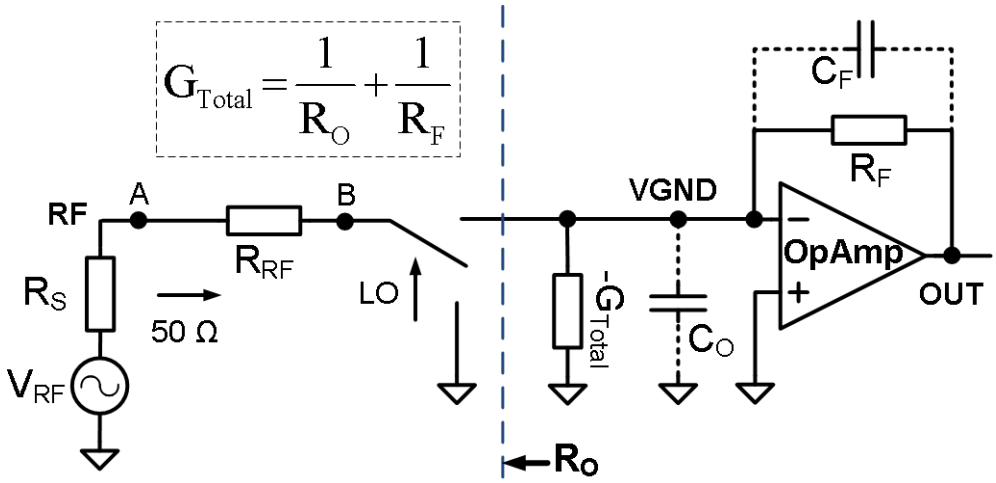

Figure 14: Replacing the LNTA (GM) of Figure 3 by a linear resistance R_{RF}

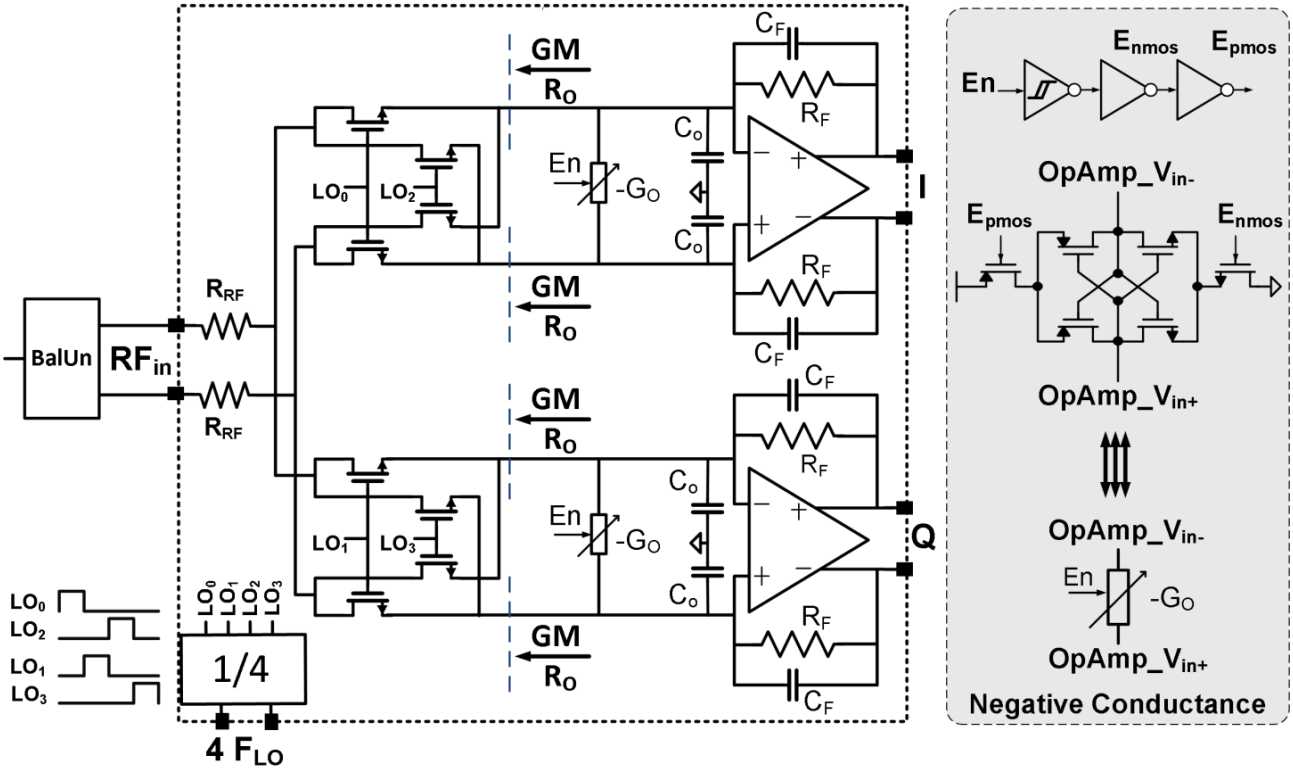

Figure 15: Complete Receiver with distortion compensation by $-G_O$

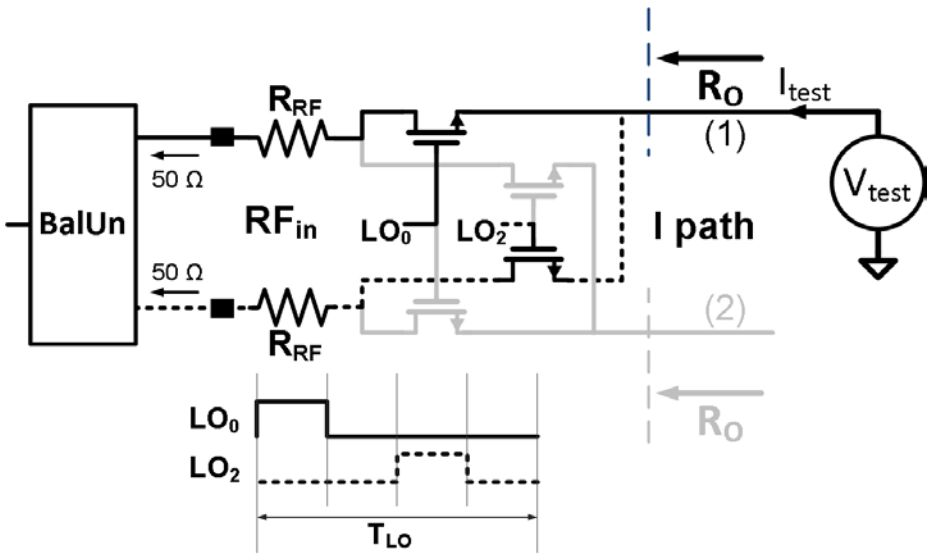

Figure 16: Derivation of R_O

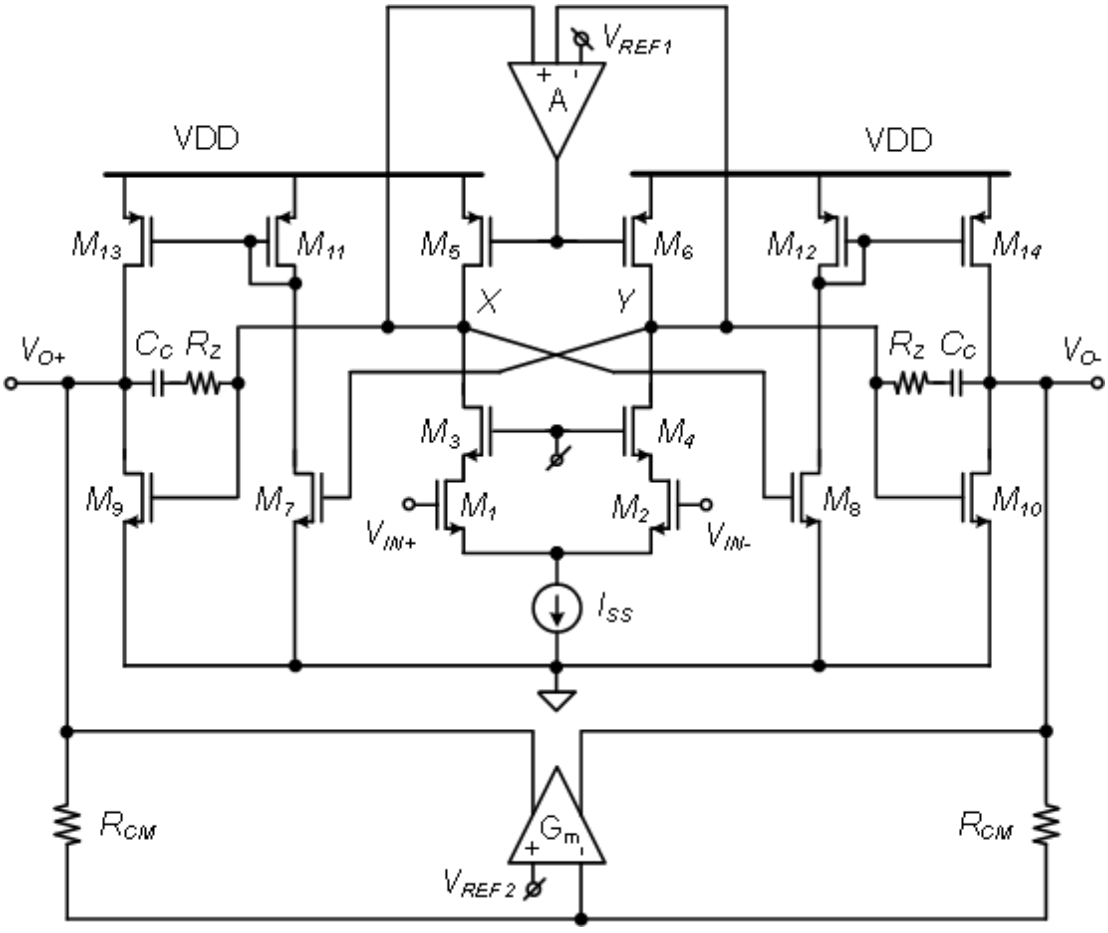

Figure 17: Circuit Diagram of the fully differential OpAmp design [12]

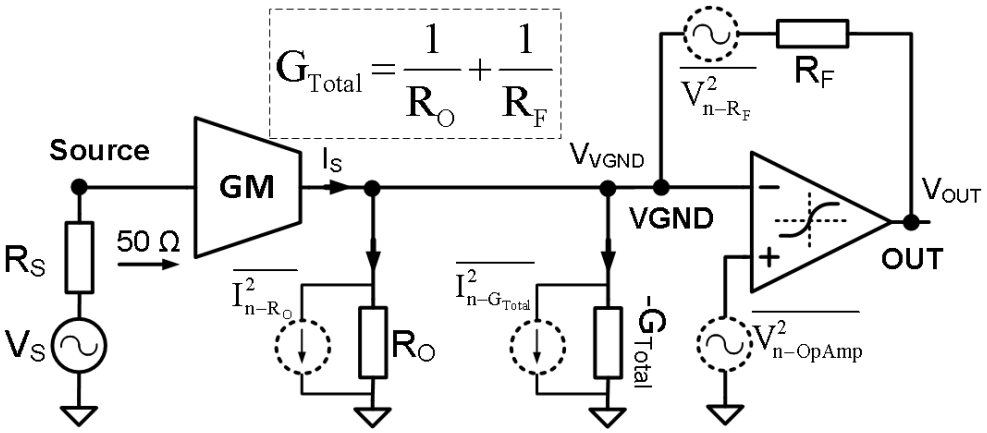

Figure 18: Equivalent baseband model for Noise Figure analysis

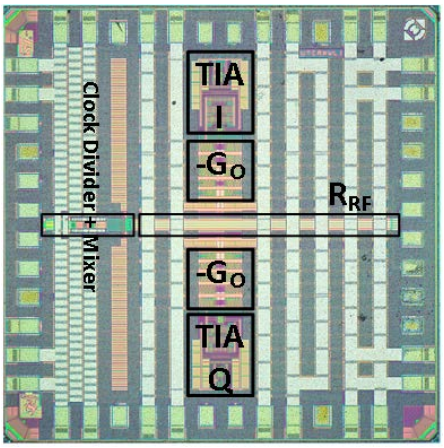

Figure 19: Die Photograph (65nm CMOS, 1.45mm x 1.45mm)

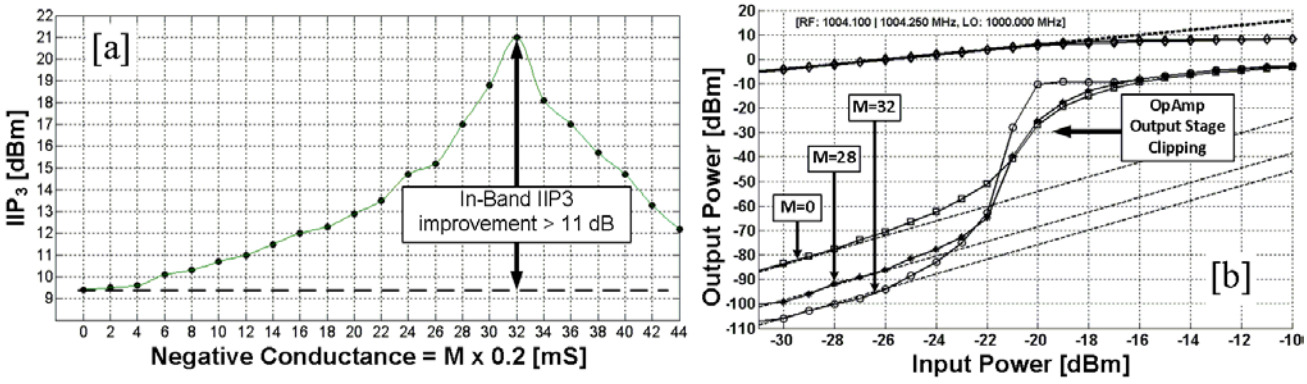

Figure 20: Measurements: (a) In-band IIP_3 vs. the number of parallel Negative Conductance Unit-Cells M (b) IM_3 versus input power for three M settings, with LO=1GHz

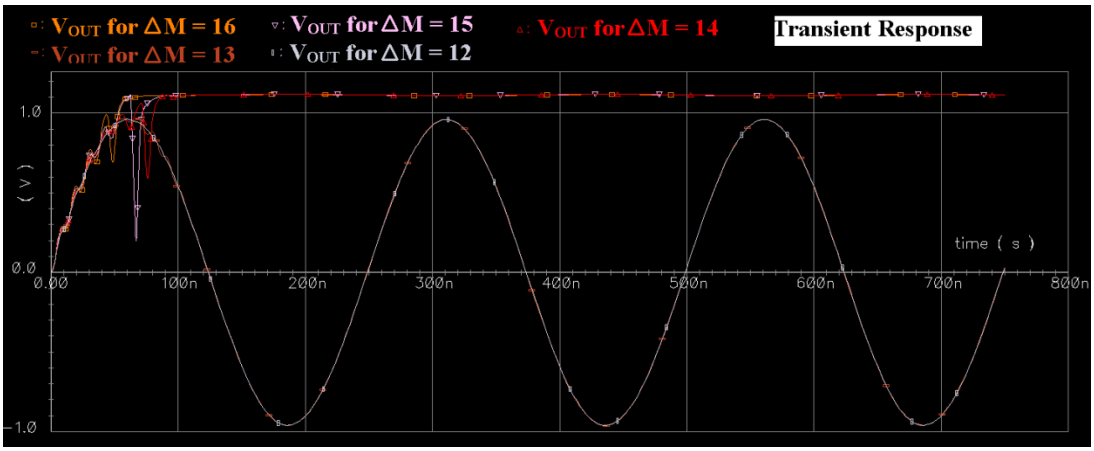

Figure 21: Latch-up simulation of V_{OUT}, input power of -16 dBm

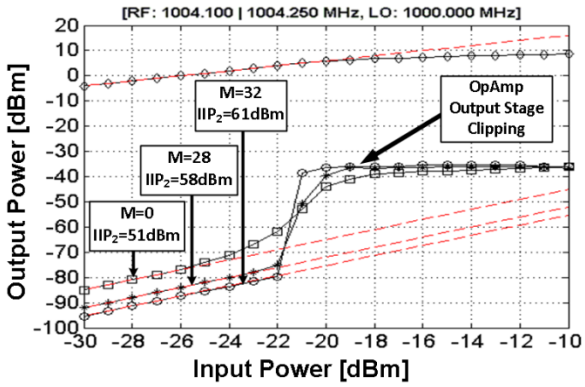

Figure 22: Measurements: IM_2 versus input power for three M settings, with LO=1GHz

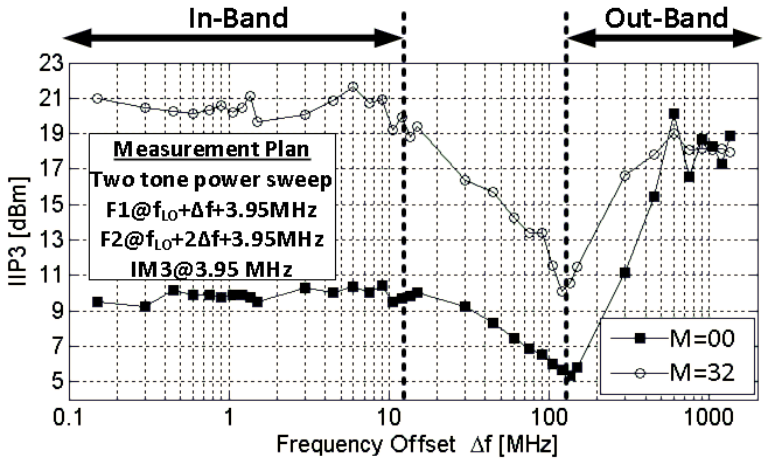

Figure 23: 2-tone IIP_3 measured at IM_3=3.95MHz versus tone spacing Δf, with LO=1GHz

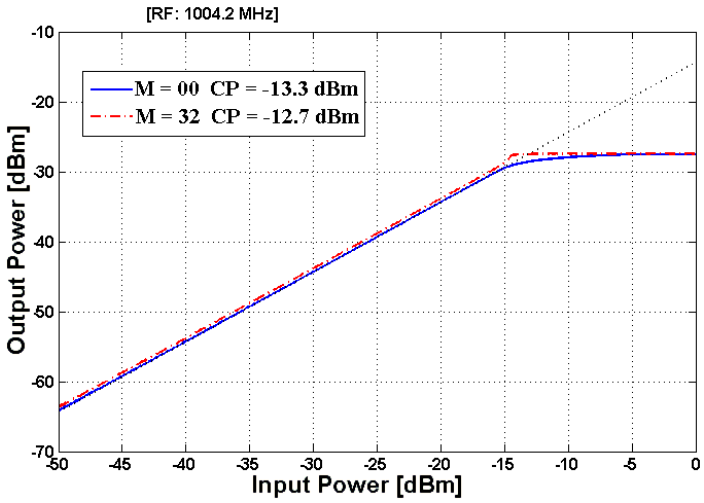

Figure 24: Compression point

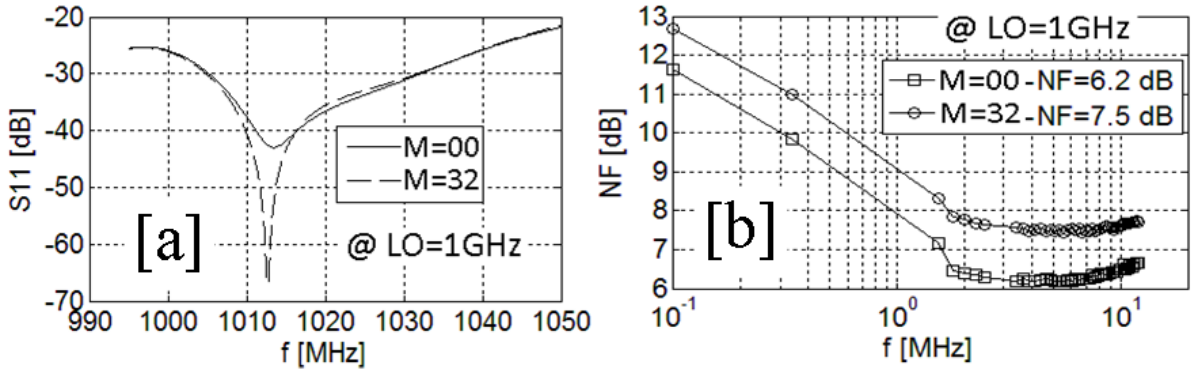

Figure 25: Measurements (a) S_{11} (b) Noise Figure, with LO=1GHz

Table I: IIP_2 and IIP_3 improvement

M	IIP2 [dBm]	IIP3 [dBm]
0	51	9.4
28	58.4	17
32	61.2	21

Table II: Summary of measurement results and comparison to other state-of-the-art receivers

	This work	Ru [3]	Murphy [4]	Youssef [5]	Soer [6]	Andrews [7]	units
Linearization Technique	Negative GO	Partial cancel Noise/Distortion	Cancel Noise	Freq. Translated Active feedback	Feedback + N-path filter	Feedback + N-path filter	
Matching	Switch-R	Common-gate	Switch-R	R	-	via TIA	
Mixer type	Switch-R	Switch-I	Switch-R&I	Gm + Switched-I	Switch-RC	Switch-RC	
Baseband-stage	TIA + RC	TIA+RC	TIA + RC	Inverter-RC	Voltage Amp	TIA+RC	
CMOS Techn.	65nm	65nm	40nm	65nm	65nm	65nm	
Active Area	< 0.2	< 1	1.2	< 0.06	< 0.13	0.75	mm2
RF Frequency	0.2-2.6	0.4-0.9	0.08-2.7	1.0-2.5	0.2-2.0	0.1-2.4	GHz
Gain	26.5	34	70	30	19	40-70	dB
In-band BW[1]	24	24	4	5	50	1.6	MHz
NF	7.5	4	2	7.25-8.9	6.5	4	dB
In-band IIP_3	**> +20**	+3.5	-22	-20	+11	-67	dBm
SFDR @ 1MHz bandwidth	**85**	75	60	57	79	29	dB
Wide-Band IIP_3 @2-tone Δf	≥+18 @ >450 >+10 @ All Δf	+18 @ Δf>800	+13.5 @Δf>40	> +12 @ Δf>60	Not measured	+25 @ Δf>50	dBm @ MHz
Supply Voltage	1.2	1.2	1.3	1.2	1.2	1.2 / 2.5	V
Power Consumption	13.9	39.6	15.6	62	60	< 70[2]	mW

[1] In-band BW is twice the zero-IF bandwidth around the LO frequency

[2] Includes the clock circuitry